Flavin-Induced Oligomerization in *Escherichia coli* Adaptive Response Protein AidB

Michael J. Hamill,[†,‡] Marco Jost,[‡] Cintyu Wong,[‡,@] Sean J. Elliott,*[,†] and Catherine L. Drennan*[,‡,§,||,⊥]

[†]Department of Chemistry, Boston University, 590 Commonwealth Avenue, Boston, Massachusetts 02215, United States
[‡]Department of Chemistry, [§]Department of Biology, [||]Howard Hughes Medical Institute, and [⊥]Center for Environmental Health, Massachusetts Institute of Technology, 77 Massachusetts Avenue, Cambridge, Massachusetts 02139, United States

Ⓢ *Supporting Information*

ABSTRACT: The process known as "adaptive response" allows *Escherichia coli* to respond to small doses of DNA-methylating agents by upregulating the expression of four proteins. While the role of three of these proteins in mitigating DNA damage is well understood, the function of AidB is less clear. Although AidB is a flavoprotein, no catalytic role has been established for the bound cofactor. Here we investigate the possibility that flavin plays a structural role in the assembly of the AidB tetramer. We report the generation and biophysical characterization of deflavinated AidB and of an AidB mutant that has greatly reduced affinity for flavin adenine dinucleotide (FAD). Using fluorescence quenching and analytical ultracentrifugation, we find that apo AidB has a high affinity for FAD, as indicated by an apparent dissociation constant of 402.1 ± 35.1 nM, and that binding of substoichiometric amounts of FAD triggers a transition in the AidB oligomeric state. In particular, deflavinated AidB is dimeric, whereas the addition of FAD yields a tetramer. We further investigate the dimerization and tetramerization interfaces of AidB by determining a 2.8 Å resolution crystal structure in space group $P3_2$ that contains three intact tetramers in the asymmetric unit. Taken together, our findings provide strong evidence that FAD plays a structural role in the formation of tetrameric AidB.
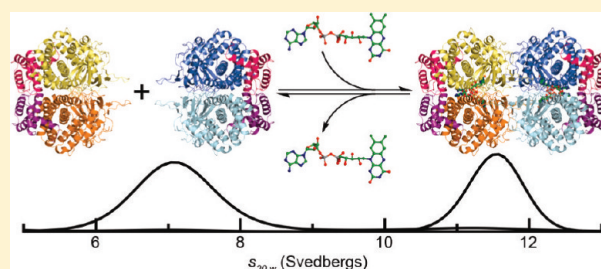
Exposure of *Escherichia coli* cells to small doses of DNA-methylating agents initiates a response that mitigates the mutagenic and cytotoxic effects of DNA methylation.[1−3] This process, known as the adaptive response, involves the upregulation of four proteins: Ada, AlkA, AlkB, and AidB.[1,4] Ada is a DNA methyltransferase that irreversibly transfers a methyl group from the DNA phosphodiester backbone to its Cys38 side chain or from O^4-methyl-T and O^6-methyl-G lesions to its Cys321 side chain.[5,6] Upon methylation at Cys38, Ada becomes a transcription factor and activates the transcription of its own encoding gene and the other adaptive response genes.[7,8] AlkA is a DNA glycosylase that repairs a variety of lesions, including 3-methyl-A, through a base excision mechanism.[9,10] The third member of the adaptive response, AlkB, is an α-ketoglutarate- and Fe(II)-dependent dioxygenase that repairs 1-methyl-A and 3-methyl-C lesions by an oxidative demethylation mechanism.[11−15] While the roles of Ada, AlkA, and AlkB in the adaptive response are well-established, AidB is still enigmatic.

Although reported to diminish the mutagenic effect of the methylating agent *N*-methyl-*N*′-nitro-*N*-nitrosoguanidine (MNNG),[16] an exact AidB phenotype has been difficult to establish. While in vitro studies clearly show protection of DNA from methylating agents such as MNNG,[17] cells with an inactivated *aidB* gene do not show the expected increase in methylation sensitivity.[2,18] Recently, it has been suggested that localization of AidB and its protective function to specific

regions of the genome could obscure the AidB phenotype, although more work is needed to fully resolve this issue.[17] Our understanding of how AidB exerts its protective function is also in its infancy. AidB is known to be a flavin adenine dinucleotide (FAD)-containing protein[19] that shares sequence homology with members of the acyl-coenzyme A dehydrogenase (ACAD) flavoenzyme family and exhibits low levels of isovaleryl-coenzyme A dehydrogenase (IVD) activity.[16] However, this activity is 1000-fold lower than that of other known ACADs, indicating that it does not represent the biological function of AidB.[19] The concomitant discovery that AidB can bind double-stranded DNA nonspecifically with low micromolar dissociation constants[19,20] led to a functional model in which AidB screens DNA and directly repairs methylated bases by a dehydrogenation reaction.[19] While there is structural and biochemical support for the presence of DNA-binding domains on AidB,[19,20] the AidB structure also shows that the four FAD binding sites per tetramer are far from these DNA-binding regions, raising doubt that AidB directly repairs DNA.[20]

In a previous crystallographic study, AidB was crystallized in the presence of DNA oligonucleotides, and although these DNA molecules were not observed in the crystal structure, the assembly of AidB molecules in the crystal lattice created 25 Å

pores lined by the DNA-binding regions of AidB.[20] On the basis of this structure, a model was put forward in which AidB sheaths DNA from destructive modification by completely sequestering it in these pores, with a potential secondary role for the FAD cofactor in detoxifying damaging agents via an unknown mechanism.[20] It was later shown that AidB can bind to certain DNA sequences with enhanced affinity during normal cell growth, including the upstream sequence of its own promoter, and that AidB plays a protective role even when its DNA-binding regions are deleted, suggesting that the purpose of the DNA binding ability of AidB is to localize detoxification activity rather than to protect DNA by providing a sheath.[21] Again, the exact nature of this putative detoxification reaction is unknown, with a recent study ruling out MNNG as an obvious substrate candidate.[22]

As outlined above, numerous models have been proposed for the role of AidB in the adaptive response. At the heart of this mystery is the role of the bound FAD. Is AidB an enzyme that uses the FAD as a cofactor for detoxification or DNA repair? Is AidB a DNA-binding protein for which the FAD plays a structural role, or could FAD play both a catalytic and a structural role in a multifaceted AidB protein? To address these questions, we investigated for the first time the properties of binding of FAD to AidB. Using a combination of techniques, we find that FAD binds tightly and cooperatively to AidB, inducing a change in the oligomeric state of the protein, from dimer to tetramer.

■ MATERIALS AND METHODS

Cloning and Site-Directed Mutagenesis. The AidB gene was amplified from *E. coli* strain AB1157 using a protocol reported previously.[19] The amplified gene was subcloned into a pET28a vector (Novagen) that had been digested with NcoI and HindIII. The resulting tag-free construct, pET28a-*wt*AidB, was transformed into *E. coli* BL21(DE3) cells for expression. An AidB triple mutant (T185V/S191R/R324D, *mt*AidB) was generated from the wild-type AidB-pET28a clone using the QuikChange Site-Directed Mutagenesis Kit (Stratagene) and the primers listed in Table S1 (Supporting Information).

Overexpression and Purification. Luria-Bertani medium (4 × 1 L) containing 50 μg/mL kanamycin was inoculated with a starter culture of *E. coli* BL21(DE3) transformed with pET28a-*wt*AidB. Cells were grown at 37 °C to an optical density of 0.5 at 600 nm, at which point the cells were induced with 1 mM isopropyl β-D-1-thiogalactopyranoside. The cultures were then transferred to 21 °C for overnight growth. Cells were harvested by centrifugation at 10000g for 10 min, and the resulting cell pellets were resuspended in AidB buffer [50 mM Tris (pH 7.8), 1 mM ethylenediaminetetraacetic acid (EDTA), 300 mM NaCl, 10% (v/v) glycerol, and 5 mM β-mercaptoethanol (β-ME)] and lysed by sonication. Cell debris was separated from the soluble supernatant by centrifugation at 35000g for 30 min at 4 °C. The cell lysate was treated with ammonium sulfate at final concentrations of 30 and 45% in a stepwise fashion. After each addition, the solution was stirred gently for 1 h at room temperature to reach equilibrium. Precipitated protein was removed by centrifugation at 6000g for 30 min at 4 °C. The protein that precipitated after the addition of 45% ammonium sulfate was separated from the supernatant and dissolved in 10 mL of AidB buffer. This solution, containing crude *wt*AidB, was loaded onto a low-substitution phenyl Sepharose column (GE Healthcare) pre-equilibrated with AidB buffer, and the column was washed with 10 column

volumes of AidB buffer. *wt*AidB was eluted with AidB buffer supplemented with 0.4% (w/v) deoxycholate. Fractions containing *wt*AidB, as judged by color and sodium dodecyl sulfate–polyacrylamide gel electrophoresis (SDS–PAGE), were merged, concentrated to 5 mL, and loaded onto a HiPrep 26/60 Sephacryl S200 size exclusion column (Amersham Bioscience) pre-equilibrated with AidB buffer. Protein was eluted with 1.5 column volumes of AidB buffer. Fractions containing pure *wt*AidB, as judged by SDS–PAGE, were merged and used for experiments within 2 days (here, "fresh" AidB is protein that is <2 days old). *mt*AidB was overexpressed and purified in the same fashion as *wt*AidB. Reduced *wt*AidB was generated by incubation of a solution of 1 mg/mL *wt*AidB in AidB buffer with a 2-fold molar excess of sodium dithionite in an oxygen-free environment (Coy Scientific chamber under a 95% Ar/5% H$_2$ atmosphere).

Deflavination. *wt*AidB (10 mL) that eluted from the Sephacryl S200 size exclusion column was diluted to a final volume of 50 mL with deflavination buffer [250 mM sodium phosphate (pH 7.5), 3 M KBr, 1 mM EDTA, 10% (v/v) glycerol, and 5 mM β-ME]. The mixture was incubated at 4 °C for 4 days, concentrated to 5 mL, and applied to a PD-10 desalting column (GE Healthcare) pre-equilibrated with deflavination buffer to remove free FAD. The amount of residual FAD was determined photometrically by the absorbance at 450 nm (ε_{450} = 11300 M^{-1} cm^{-1} [19]), and the deflavination process was repeated if necessary. The final apo *wt*AidB sample was buffer exchanged with AidB buffer using a PD-10 column. UV–vis spectra of apo *wt*AidB were recorded on a Cary 50 Bio spectrophotometer (Varian).

Circular Dichroism Spectroscopy. Circular dichroism spectra were recorded on an Aviv 62 DS circular dichroism spectrometer at 25 °C using a 0.1 cm optical path length cell. The protein concentration was 1.2 mg/mL in a buffer containing 200 mM potassium phosphate (pH 7.5), 1 mM EDTA, 10% (v/v) glycerol, and 5 mM β-ME. Ellipticity was recorded from 200 to 240 nm in 1 nm steps with a 20 s averaging time and a 1.5 nm bandwidth. At least three scans were averaged for each sample. Mean residue ellipticity, θ in degrees square centimeters per decimole, was calculated from the equation θ = MRW × θ_{obs}/(10dc), where θ_{obs} is the observed ellipticity measured in degrees, MRW is the mean residue molecular mass (112.0 Da), c is the protein concentration in grams per milliliter, and d is the optical path length of the cell in centimeters.[23]

Fluorescence Quenching. The affinity of apo *wt*AidB for free FAD was determined by monitoring the extent of fluorescence quenching[24] at 20 °C, using a SpectraMax M2 microplate reader (Molecular Devices). Fluorescence emission of FAD was detected at 520 nm with excitation at 350 nm. Fresh apo *wt*AidB (200 nM to 5 μM) and 1 μM FAD, each in AidB buffer, were mixed by being shaken for 2 min. Fluorescence was recorded over time until equilibrium was reached. The change in fluorescence intensity as a function of binding of apo *wt*AidB to FAD was fit to the Hill equation (eq 1), which accounts for cooperative binding:

$$\frac{\Delta F}{\Delta F_{max}} = \frac{[\text{AidB}]^h}{K_d{}^h + [\text{AidB}]^h} \quad (1)$$

where ΔF is the change in FAD fluorescence at 520 nm at each AidB concentration, ΔF_{max} is the change in fluorescence at 520 nm at a saturating *wt*AidB concentration, K_d is the dissociation

constant, h is the Hill coefficient, and [AidB] is the concentration of wtAidB.

Analytical Ultracentrifugation. Sedimentation velocity experiments were performed using a Beckman Coulter Optima XL-I analytical ultracentrifuge equipped with a Beckman An60Ti rotor and an XL-A monochromator. Absorbance data were collected at 280, 350, or 385 nm, 20 °C, and 30000 rpm until sedimentation was complete. All experiments were performed with at least two different protein samples. The protein concentrations for the different samples were 9.0 and 9.6 μM for holo wtAidB, 6.1 and 16.7 μM for apo wtAidB, 7.0 and 8.5 μM for apo mtAidB, 6.8 and 16.7 μM for reconstituted wtAidB, and 7.4 and 7.4 μM for reduced wtAidB. All protein samples were freshly prepared in AidB buffer. For reduced wtAidB, the protein solution and the analytical ultracentrifugation cells were handled in an oxygen-free environment (Coy Scientific chamber under a 95% Ar/5% H_2 atmosphere) until the cells were sealed from air. Stoichiometric reconstitution experiments were performed by incubation of apo wtAidB with free FAD at 4 °C for 16 h. For the following sedimentation velocity experiments, the FAD absorbance at 385 nm was simultaneously monitored along with the absorbance at 280 nm. The density and viscosity of the buffer solution at 20 °C were calculated with Sednterp, which uses formulae based on a database of known values.[25] Hydropro was used to calculate theoretical AidB hydrodynamic properties,[26] based on a hydrodynamic model created from our AidB crystal structure. The distribution of sedimentation coefficients was calculated by fitting sedimentation velocity data using Sedfit.[27] For this analysis, the continuous distribution $c(s)$ Lamm equation model was used, which accounts for protein diffusion.[27] All Sedfit sedimentation coefficient results were confirmed by additional $g^*(s)$ analysis using DCDT+.[28]

Fluorescence Anisotropy. Fluorescence anisotropy experiments were performed using a SpectraMax M5 microplate reader (Molecular Devices) as described previously.[20] The oligonucleotide consisted of a 28-mer of DNA that is known to bind to AidB (UP element with the −35 box of the rrnB P1 promoter) and contained a fluorescein label at the 5′-end: 5′-fluorescein-GAAAATTATTTTAAATTTCCTCTTGTCA-3′ and 5′-TGACAAGAGGAAATTTAAAATAATTTTC-3′.[17] Polarized fluorescence was monitored using excitation and emission wavelengths of 495 and 538 nm, respectively. Samples of 50 nM fluorescein-labeled DNA in AidB buffer were mixed with 0−20 μM holo or apo wtAidB or apo mtAidB, in agreement with conditions used previously.[20] Anisotropy was measured after equilibrium was reached. Binding curves were fit to a two-state binding model to determine K_d as follows:

$$r = (r_{max} - r_0)\left(\frac{[\text{AidB}]}{K_d + [\text{AidB}]}\right) + r_0 \tag{2}$$

where r_0 is the anisotropy of labeled DNA, r_{max} is the anisotropy at saturating concentrations of AidB, K_d is the dissociation constant, and [AidB] is the concentration of AidB.

Crystallization of AidB and Data Collection in the $P3_2$ Crystal Form. wtAidB was crystallized at 25 °C by the hanging drop vapor diffusion technique; 1 μL of a protein solution [10 mg/mL wtAidB in 10 mM Tris (pH 7.8), 100 mM NaCl, 10% (v/v) glycerol, and 2 mM β-ME] was mixed with 1 μL of a precipitant solution [100 mM HEPES (pH 7.5), 20% (v/v) ethanol, and 200 mM $MgCl_2$] on a coverslip and sealed over 0.5 mL of precipitant solution. Trigonal crystals with

dimensions of ∼0.3 mm × 0.2 mm × 0.1 mm appeared within 2 weeks. Crystals were flash-frozen in liquid nitrogen without the use of additional cryoprotectants.

All crystals belonged to space group $P3_2$. Data were collected to 2.8 Å resolution at the Advanced Photon Source (Argonne, IL) on beamline 24ID-C using an ADSC Q315 detector. All data were collected at 100 K. Data were reduced in Denzo and scaled using Scalepack.[29] Data collection statistics are summarized in Table S2 of the Supporting Information.

Determination and Refinement of the $P3_2$ Crystal Structure of AidB. The structure of wtAidB was determined by molecular replacement in Phaser[30] using data to 2.8 Å resolution. The search model was the published structure of wtAidB (Protein Data Bank entry 3DJL[20]) without any cofactor or water atoms. The best rotational and translational solution had a correlation coefficient of 26.9 with 12 wtAidB protomers per asymmetric unit, corresponding to three tetramer units related by noncrystallographic symmetry (NCS). The resulting model was subjected to rigid body refinement followed by simulated annealing refinement in CNS.[31,32] After the first round of refinement, R_{cryst} and R_{free} were 31.9 and 31.5%, respectively. Cofactors, ions, and a modest number of water molecules were added to the model at 2.8 Å resolution followed by iterative rounds of model building in Coot[33] and refinement in PHENIX.[34] NCS restraints were applied across the six wtAidB dimers in the asymmetric unit to reduce the number of variables in the refinement as opposed to applying NCS restraints across wtAidB tetramers. Residues involved in crystal lattice contacts were excluded from NCS restraints. The final cycles of refinement included TLS parametrization using one TLS group per tetramer.[35] In all chains, either residues 2−540 or residues 1−540 were observed out of a total of 541 residues. In addition, each chain contained one molecule of FAD, one chloride ion, and a disulfide bridge between Cys28 and Cys540. Simulated annealing composite omit maps calculated in CNS were used to validate the model.[31,32] The final structure was refined to 2.8 Å resolution with R_{cryst} and R_{free} values of 20.4 and 22.9%, respectively. The resulting model exhibited excellent stereochemistry and small root-mean-square deviations from ideal values for bond lengths and bond angles; 0.1% of the residues are in disallowed regions of the Ramachandran plot. For most of the outliers, the backbone is involved in FAD binding, possibly providing stabilization for less favorable backbone conformations. Refinement statistics for the final model are summarized in Table S3 of the Supporting Information. The geometry of the final model was analyzed using MolProbity.[36] Figures were generated in PyMOL.[37]

■ RESULTS

Preparation and Spectroscopic Analysis of Deflavinated AidB. To investigate the role of the bound flavin cofactor, we generated deflavinated AidB (apo AidB) both by a chemical method using KBr (apo wtAidB) and by creating a flavin-binding deficient triple mutant (T185V/S191R/R324D) of AidB (apo mtAidB). Whereas deflavination by typical treatments, such as dialysis and chromatography,[38] was unsuccessful with AidB, dilution of fresh wtAidB into a buffer containing KBr, a chaotropic agent that competes with the flavin for the phosphate binding site, quantitatively yielded apo wtAidB. To generate a mutant form of AidB with greatly reduced FAD affinity, we inserted the T185V, S191R, and R324D mutations into the sequence of wtAidB. All three of these residues are directly involved in FAD binding (Figure S1

of the Supporting Information). During the size exclusion chromatography step of the protein purification procedure, the resulting triple mutant *mt*AidB eluted as two species. A minor species with a shorter retention time exhibited a bright yellow color, indicative of bound FAD, while the major species was colorless and appeared to be deflavinated. Because we did not overexpress our mutant protein in an *aidB* knockout strain, the minor species most likely represents endogenous AidB while the major species is our overexpressed mutant protein.

To ensure deflavination of all samples used in these experiments, we analyzed both apo *wt*AidB and apo *mt*AidB by UV−vis spectroscopy. The characteristic FAD absorption features were not observed in either apo *wt*AidB or apo *mt*AidB, indicating that no or very little FAD was present in either sample (Figure S2A of the Supporting Information). We then performed circular dichroism (CD) spectroscopy on holo *wt*AidB, apo *wt*AidB, and apo *mt*AidB to assess whether the deflavinated protein was properly folded. The CD spectra of apo *wt*AidB and apo *mt*AidB were almost identical to that of holo *wt*AidB, with no deviations above background (Figure S2B of the Supporting Information). Upon stoichiometric reconstitution of apo *wt*AidB with FAD, the absorption features were restored and the CD spectrum remained unchanged. Therefore, we concluded that we achieved deflavination without major structural perturbations and used these deflavinated species for further analyses.

wtAidB Binds FAD Tightly and Cooperatively. To investigate the interaction of FAD with *wt*AidB, we measured the dissociation constant (K_d) by fluorescence quenching (Figure 1). FAD has a fluorescence emission band centered at
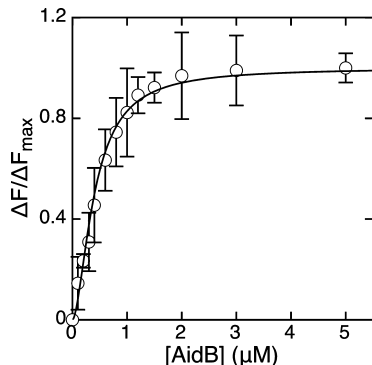

Figure 1. Quenching of FAD fluorescence upon binding to apo *wt*AidB. Plotted is the ratio between the change in FAD fluorescence at each *wt*AidB concentration (ΔF) and the change in fluorescence at saturating *wt*AidB concentrations (ΔF_{max}) vs the concentration of *wt*AidB. The data were fit to the Hill equation (eq 1). Data points and error bars represent the average of three experiments.

520 nm when it is excited at 350 nm. When FAD binds to *wt*AidB, the fluorescence emission of FAD at 520 nm is quenched by a factor of 3.1. Binding data were fit to a Hill equation (eq 1) to account for cooperative binding. Because cooperativity implies multiple and unequal binding equilibrium states, the resulting K_d is a rough estimation of the average dissociation constant. We calculate an apparent K_d of 402.1 ± 35.1 nM with a Hill coefficient (h) that is greater than 1 (1.73 ± 0.21), consistent with tight and cooperative binding of FAD to *wt*AidB.

The Oligomeric State of AidB Is Flavin-Dependent. We performed sedimentation velocity analytical ultracentrifugation

(AUC) experiments to determine the oligomeric state of AidB under different conditions. Sedimentation velocity data were fit to a continuous distribution $c(s)$ Lamm equation model using Sedfit,[27] yielding the experimental sedimentation coefficient distribution. All sedimentation coefficients, which are dependent on the mass and shape of the protein, were normalized to 20 °C in water ($s_{20,w}$). We also used Hydropro[28] to determine theoretical $s_{20,w}$ values for different oligomers of AidB based on our crystal structure (see below). The calculated $s_{20,w}$ value for the putative AidB tetramer was 11.5 S. In contrast, the $s_{20,w}$ values for possible dimer combinations ranged between 6.4 and 7.0 S, and the $s_{20,w}$ value for an AidB monomer was 4.2 S. These values were compared to experimentally determined $s_{20,w}$ values, allowing us to assign oligomeric states to the different AidB samples.

First, we collected AUC data on holo *wt*AidB, apo *wt*AidB, and apo *mt*AidB to assess the influence of the FAD cofactor on the oligomeric state. For holo *wt*AidB, we obtained an experimental $s_{20,w}$ value of 11.5 S (Figure 2A), indicative of a tetramer structure and in agreement with previously reported results.[19,20] Trace amounts of smaller species (asterisks in Figure 2A) likely represent a small amount of misfolded, denatured, or monomeric protein. In contrast, the major species of apo *wt*AidB exhibited an $s_{20,w}$ value of 7.0 S, indicating that apo *wt*AidB is a dimer (Figure 2B). Small amounts of a tetrameric species are observed in the sample, but the ratio of dimer to tetramer did not change with a 2.7-fold increase in protein concentration. For apo *mt*AidB, we obtained an $s_{20,w}$ value of 7.1 S for the dominant species (Figure 2C), in close agreement with the value obtained for apo *wt*AidB. Thus, both deflavinated AidB species are dimeric in solution, indicating that AidB undergoes a change in the oligomerization state, from a tetramer to a dimer, upon removal of the FAD cofactor.

Using a stepwise reconstitution protocol of apo *wt*AidB with free FAD, we then tested whether the observed changes in oligomerization state are reversible. FAD was added to apo *wt*AidB at molar ratios of 0.25, 0.5, and 1.0 with respect to the concentration of the AidB monomer. The samples were then subjected to AUC with simultaneous monitoring of the absorbance at both 280 and 385 nm (Figure 2D−F). Sedimentation coefficients of the various forms of AidB were calculated from the absorbance at 280 nm (Figure 2D-F, top traces), while the absorbance at 385 nm was used to identify FAD-containing AidB (Figure 2D-F, bottom traces). Upon reconstitution of apo *wt*AidB with 0.25 equiv of FAD, we observed a species with an $s_{20,w}$ value of 11.5 S in the AUC experiment, accounting for 47% of the total AidB (Figure 2D). A second species exhibited an $s_{20,w}$ value of 7.0 S, accounting for the remaining AidB. The absorbance at 385 nm was observed only in the species with an $s_{20,w}$ value of 11.5 S. Thus, 47% of the AidB in solution had formed a tetramer, and all FAD was bound to this tetrameric species; no FAD was bound to a dimeric species that was also present in solution. When we increased the amount of FAD to 0.5 equiv relative to the concentration of AidB monomer, 77% of AidB was present in a tetrameric state. Again, FAD was only observed in those tetramers (Figure 2E). Finally, reconstitution using 1 equiv of FAD relative to AidB monomer resulted in 95% tetramer formation, a value similar to that observed for holo *wt*AidB (Figure 2F). All in all, these results suggest the presence of an FAD-dependent equilibrium between the dimeric and tetrameric states of AidB in which binding of FAD induces a transition to the tetramer.
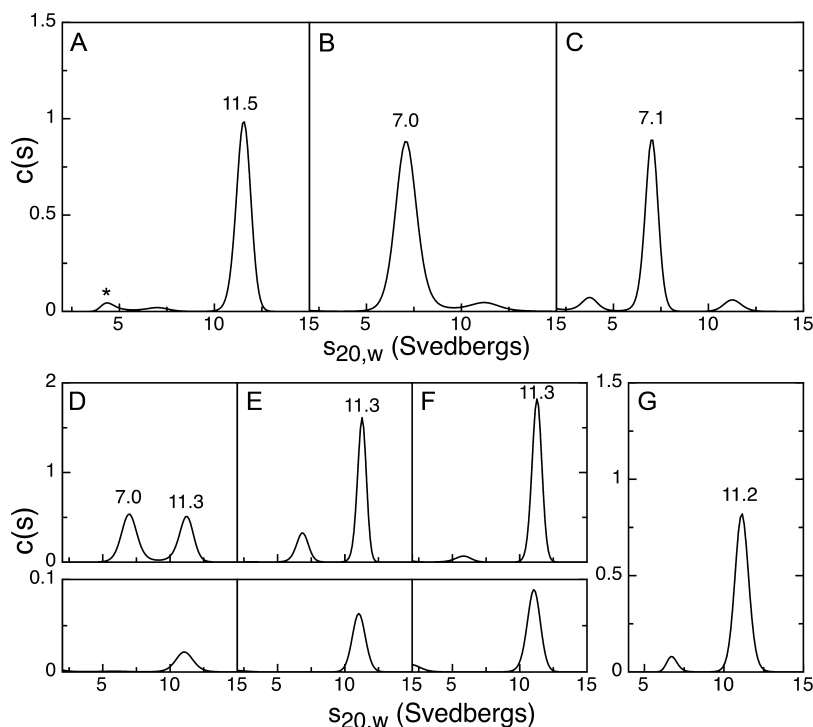
Figure 2. Sedimentation coefficient distributions for different AidB samples, showing the effect of FAD on AidB oligomeric state: (A) holo *wt*AidB, (B) apo *wt*AidB, (C) apo *mt*AidB, (D) apo *wt*AidB reconstituted with 0.25 equiv of free FAD, (E) apo *wt*AidB reconstituted with 0.5 equiv of free FAD, (F) apo *wt*AidB reconstituted with 1.0 equiv of free FAD, and (G) reduced holo *wt*AidB. For panels D–F, the distribution in the top panel is calculated from 280 nm absorbance and the distribution in the bottom from the FAD absorbance at 385 nm. Minor species observed (marked with asterisks) are likely the result of misfolded, denatured, or monomeric protein.

We also examined whether the oxidation state of the flavin cofactor had an effect on the oligomeric state of *wt*AidB. We generated *wt*AidB in complex with its reduced flavin cofactor by chemical reduction of holo *wt*AidB with a 2-fold molar excess of sodium dithionite in an oxygen-free environment. Reduced *wt*AidB exhibited an $s_{20,w}$ value of 11.2 S (Figure 2G), indicating that reduced *wt*AidB is a tetramer. We confirmed that the flavin cofactor remains in the reduced state during the time course of an AUC experiment by collecting UV–vis spectra in an oxygen-free environment after the experiment, which indicated the absence of the oxidized flavin cofactor in the sample (data not shown). Furthermore, we monitored the absorbances at 280, 350, and 385 nm in a separate anaerobic AUC experiment. All three traces exhibited the same profile: the absorbances at 350 and 385 nm remained the same over the time course of the experiment, indicating that there was no change in the oxidation state of the cofactor (data not shown). Thus, while removal of the flavin cofactor has a significant impact on the oligomerization state of *wt*AidB, holo *wt*AidB is a tetramer regardless of the oxidation state of the flavin cofactor.

Interaction between DNA and Apo AidB. To estimate the effect of deflavination on the DNA binding capability of *wt*AidB, we measured the affinity of holo *wt*AidB, apo *wt*AidB, and apo *mt*AidB for DNA by fluorescence anisotropy. In our binding studies, a specific *E. coli* DNA fragment (5′-GAAAATTATTTTAAATTTCCTCTTGTCA-3′) was chosen because AidB offers enhanced protection from damage to this DNA sequence.[17] We first determined the K_d of this oligonucleotide and holo *wt*AidB to be 2.2 ± 0.1 μM under conditions similar to those used previously (data not shown).[20] This interaction is approximately 2-fold stronger than the interaction between holo *wt*AidB and a fluorescein-tagged

random 25-mer of DNA used in previous experiments (K_d = 4.3 ± 0.1 μM).[20] We also measured the effect of ionic strength on AidB–DNA affinity by lowering the NaCl concentration from 300 to 100 mM. As expected, tighter binding (K_d = 463 ± 48 nM) between holo *wt*AidB and DNA is observed at the lower salt concentration (Figure 3). Under these low-salt

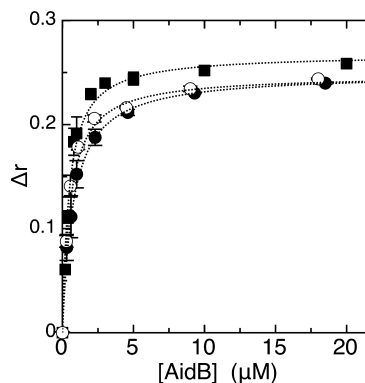**Figure 3.** Interaction between a fluorescein-labeled DNA 28-mer and holo *wt*AidB (■), apo *wt*AidB (○), and apo *mt*AidB (●). Δr is the change in fluorescence anisotropy observed upon addition of AidB. Dotted lines are the curve fits according to eq 2. Data points and error bars represent the average of three experiments.

conditions, both forms of apo AidB have similar though nonidentical DNA affinities compared to each other and to holo *wt*AidB. The K_d for the interaction of apo *mt*AidB and DNA is 763 ± 66 nM, and the K_d for the interaction of apo *wt*AidB and DNA is 548 ± 20 nM (Figure 3). Thus, although
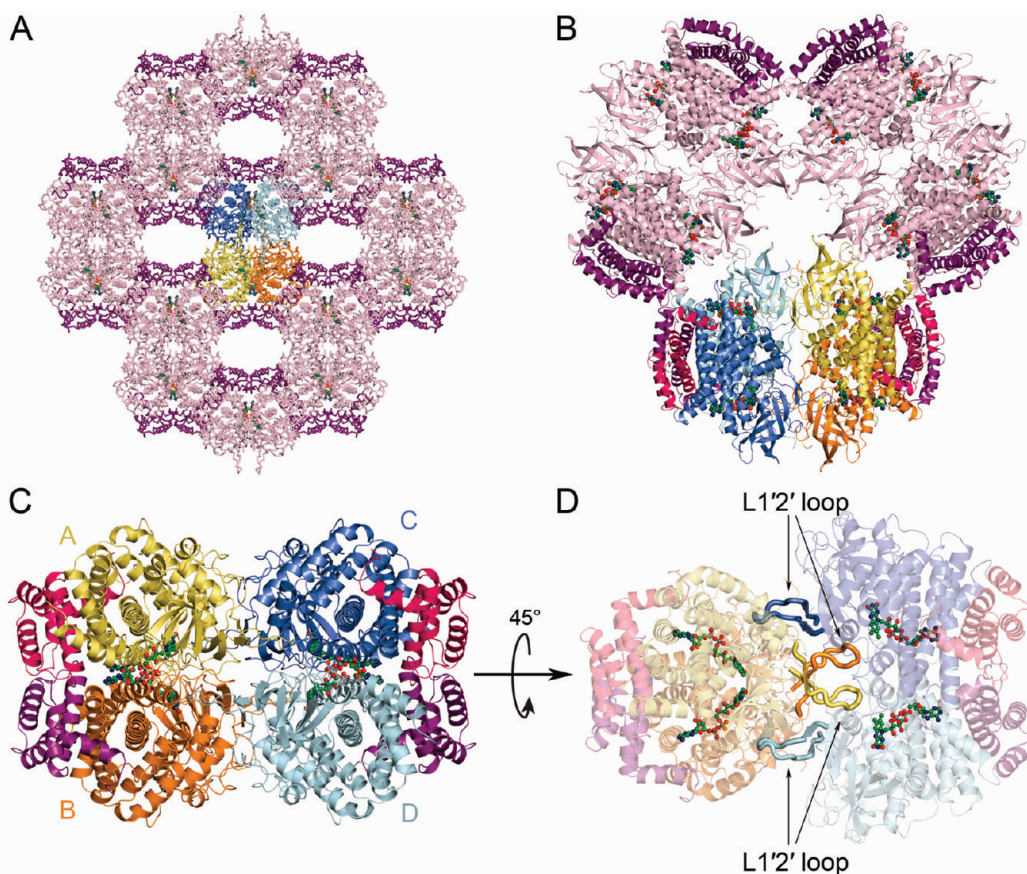
Figure 4. Crystal structures of holo *wt*AidB. (A) Higher-order oligomer of AidB observed in the *I*222 crystal structure,[20] with the central AidB tetramer colored by protomer as described below. (B) Three AidB tetramers in the asymmetric unit of the *P*3$_2$ crystal structure, with the bottom AidB tetramer colored by protomer. (C) Tetramer of holo *wt*AidB with protomers labeled A−D. (D) Tetramer of holo *wt*AidB, rotated by 45° with respect to panel C. Ribbons are transparent to emphasize the bound FAD molecules and the L1'2' loops of each protomer (thicker ribbons, marked by arrows). The general coloring scheme was as follows: protomers in a tetramer colored yellow (A), orange (B), cyan (C), and blue (D). Additional tetramers are colored pink. The putative DNA-binding regions of AidB are highlighted in purple and magenta. Bound FAD molecules are shown in ball-and-stick representation with carbon atoms colored green.

there is a significant change to the oligomerization state upon deflavination of AidB, we find the effect on DNA binding to be negligible.

P3$_2$ Crystal Structure of the AidB Tetramer. To investigate the molecular basis of the FAD-dependent changes in the AidB oligomerization state, we determined the crystal structure of holo *wt*AidB in space group *P*3$_2$ to 2.8 Å resolution (Figure 4B−D). Unlike the previous *I*222 structure,[20] this crystal form has three tetramers of AidB in the asymmetric unit as opposed to a single monomer. The *P*3$_2$ structure was determined by molecular replacement using the *I*222 crystal structure.[20] Protomers from the two crystal structures superimpose with a root-mean-square deviation (rmsd) of 0.34 Å over 538 C$_\alpha$ atoms, indicating that the structures of *wt*AidB protomers are unchanged. Also, the *wt*AidB tetramer from the *P*3$_2$ structure and the AidB tetramer generated by symmetry from the *I*222 structure superpose well, with an rmsd of 0.40 Å over 2152 C$_\alpha$ atoms. However, there are profound differences in the crystal packing arrangement of these tetramers (Figure 4A,B). The previous structure contained a crystal lattice in which four AidB tetramers form another higher-order oligomer, with the AidB DNA-binding regions lining a central pore with a 25 Å diameter (Figure 4). In the *P*3$_2$ crystal structure, the three tetramers in the asymmetric unit are arranged in a triangular shape with the DNA-binding domains pointing

outward and no obvious pore (Figure 4B). Even when considering symmetry-related molecules in the *P*3$_2$ crystal lattice, the resulting arrangement does not reveal a central pore with which AidB could sequester DNA (Figure S3 of the Supporting Information). Thus, although the tetramer of AidB is conserved in both crystal forms, the assembly of those tetramers into higher-order oligomers is not.

Structural Basis for Flavin-Dependent Oligomerization. In the *P*3$_2$ crystal structure, each protomer of an AidB tetramer interacts with each of the other protomers. Thus, there are three different types of dimers that could be formed upon deflavination: "up and down" (AB or CD dimers), "side by side" (AC or BD dimers), and "diagonal" (AD or BC dimers) (Figure 5). To investigate which of the three possible dimers of AidB is present after deflavination, we calculated theoretical $s_{20,w}$ values for each of the dimers from our crystal structure and compared these values to the results from our AUC experiments. We obtained theoretical $s_{20,w}$ values of 7.0, 6.6, and 6.4 S for the AB dimer, the AC dimer, and the AD dimer, respectively. These values reflect their differences in shape, as the AB dimer would be more globular while the AC and the AD dimers would be more elongated (Figure 5). Our observed $s_{20,w}$ values for apo *wt*AidB and apo *mt*AidB are 7.1 and 7.0 S, respectively, consistent with the value calculated for the AB dimer of 7.0 S.
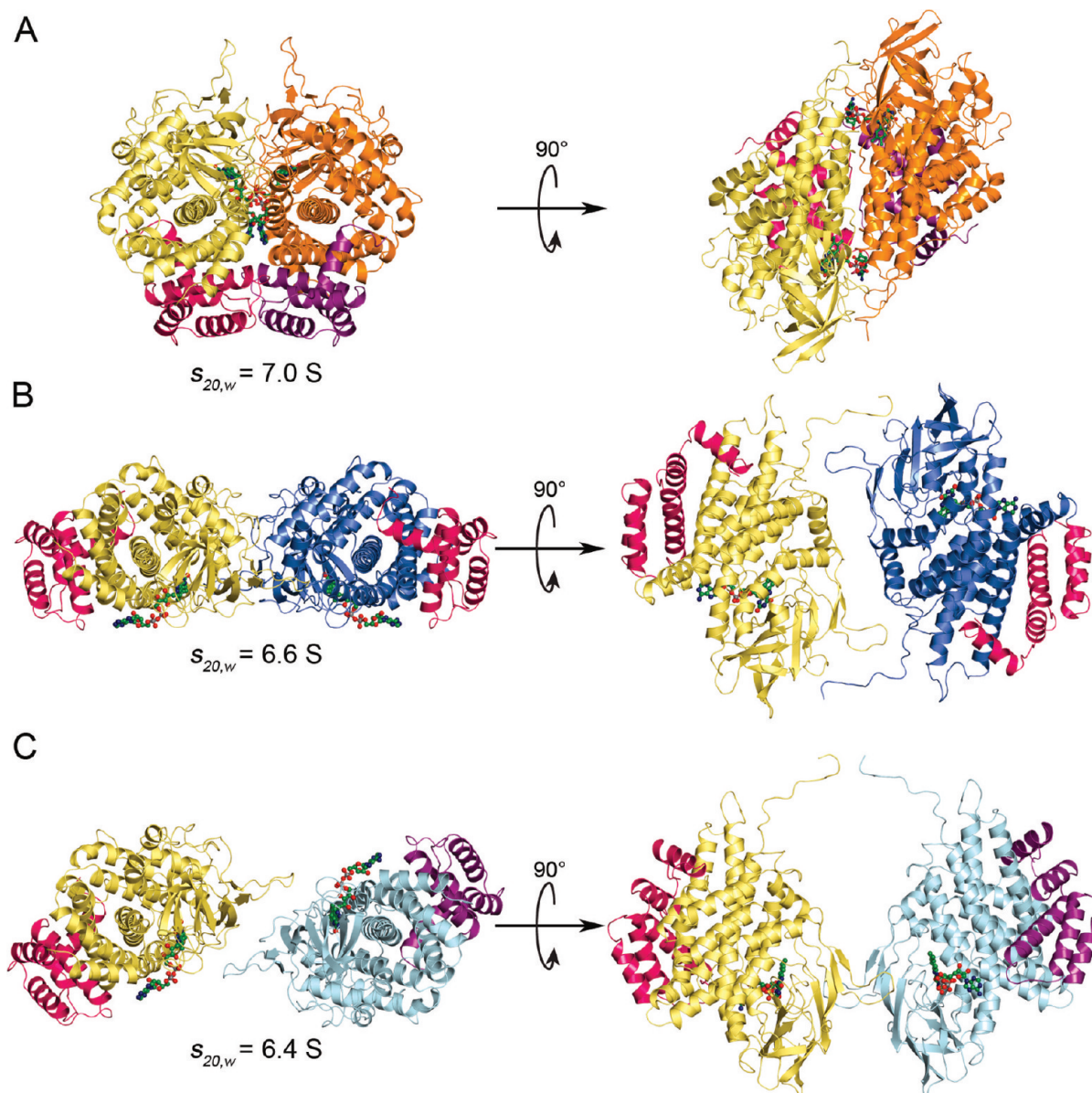
Figure 5. Dimer interfaces within holo *wt*AidB: (A) AB dimer, (B) AC dimer, and (C) AD dimer of *wt*AidB shown as ribbons. Protomers A−D of AidB are colored yellow, orange, blue, and cyan, respectively, with the DNA-binding regions colored magenta and purple. Bound FAD molecules are shown in ball-and-stick representation with carbon atoms colored green. Calculated $s_{20,w}$ values are given for each dimer.

In the $P3_2$ crystal structure, the AB dimer is held together by an extensive interface, burying a combined area of more than 6500 Å^2 from solvent (Figure 5A). The dimer interface features 33 hydrogen bonds and 24 salt bridges. In contrast, the AC and AD dimer interfaces have solvent-buried areas of only 1782 and 1319 Å^2, respectively (Figure 5B,C), providing an additional rationale for the presence of an AB dimer in solution. The FAD of each protomer is bound at the AB dimer interface, with both protomers contributing to the binding of FAD (Figure 6A). FAD is bound by 12 hydrogen bonds from one protomer, while the second protomer adds another two hydrogen bonds and two salt bridges to binding of the pyrophosphate moiety and the adenine ring (Figure 6A). In contrast, FAD makes no direct contacts across the AC or AD interfaces.

The AidB tetramer, as observed in both crystal structures, is a dimer of dimers with three 2-fold symmetry axes (Figure 4C,D). The combined buried surface area between the AB and the CD dimers is 5700 Å^2, and we refer to this interface as the "tetramer interface". With 37 hydrogen bonds and 10 salt bridges at this interface, the size of the buried surface area (7.3% of the total surface area) and the number of specific stabilizing interactions are small compared to the overall size of the putative assembly. When the tetramer interface is treated as a single interface between two polypeptide chains, the complexation significance score determined by the PISA server for interface analysis[39] is extremely low, 0.086 on a scale from 0 (lowest significance) to 1 (highest significance). Furthermore, the free enthalpy of formation is calculated to be 12.3 kcal/mol for this interface, rendering interface formation energetically unfavorable. These analyses would suggest that the interface is not significant for complex formation and is instead an artifact of crystal packing. Nonetheless, our AUC data provide conclusive evidence that holo *wt*AidB is indeed a tetramer in solution.

As described previously,[20] tetramer formation is mainly mediated by the N-termini and the L1′2′ loops (residues 69−80)
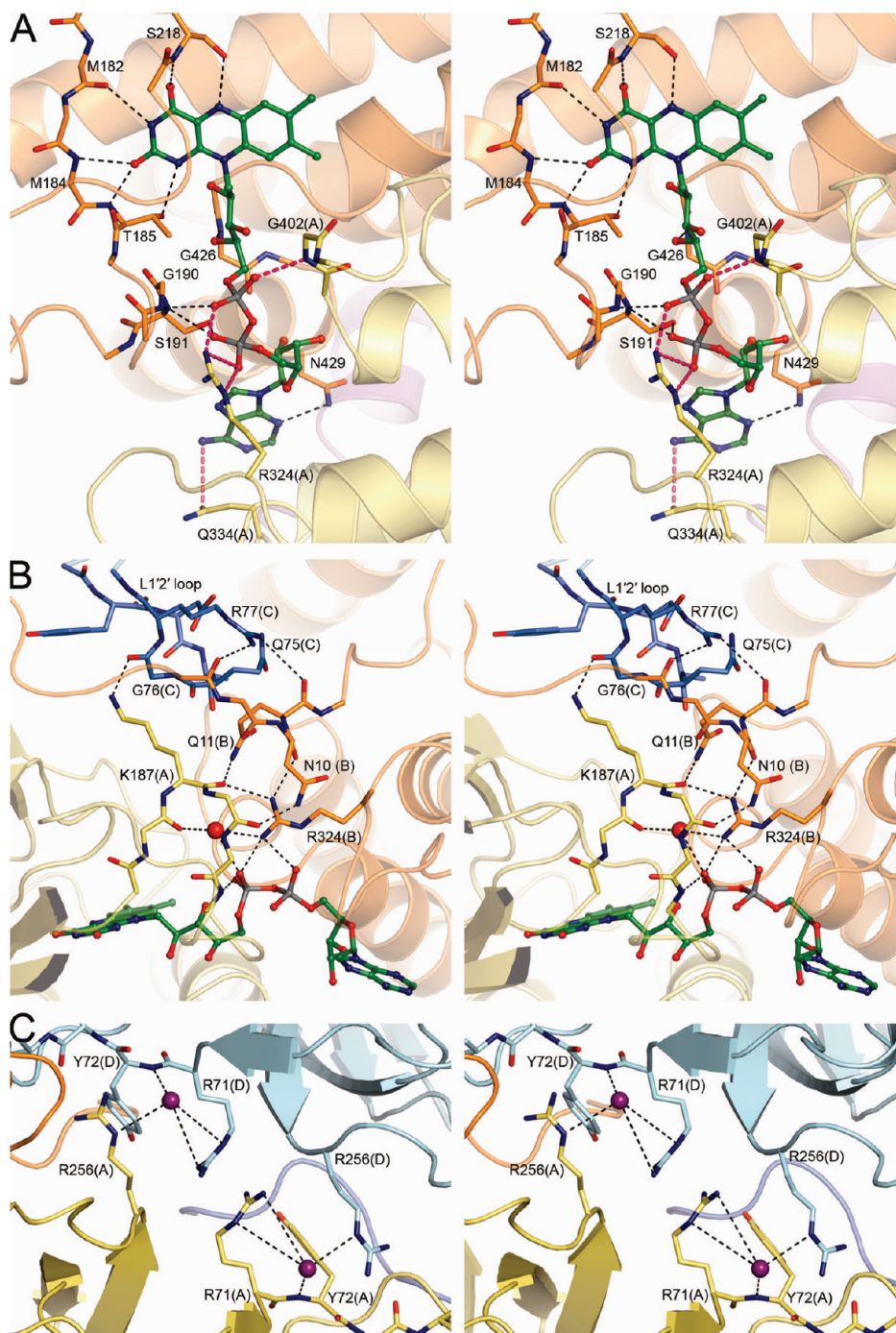
Figure 6. Involvement of FAD and chloride at interfaces of holo *wt*AidB. (A) Wall-eyed stereoview of the bound FAD cofactor at the AB dimer interface of AidB, with coloring as in Figure 4. Residues interacting directly with the FAD are shown as sticks, colored according to their corresponding protomer. Hydrogen bonding and ionic interactions between the FAD cofactor and its corresponding protomer are represented as black dashed lines, while interactions between the cofactor and the opposite protomer are represented as magenta dashed lines. Residues of the opposite protomer are labeled with their protomer in parentheses. Side chains not involved in specific contacts have been truncated for the sake of clarity. (B) Wall-eyed stereoview of the tetramer interface and the nearby FAD cofactor, with coloring as in Figure 4. Residues involved in interactions at the interface are shown as sticks, colored and labeled according to their corresponding protomer. Water molecules are shown as red spheres. Hydrogen bonding and ionic interactions are represented as black dashed lines. (C) Wall-eyed stereoview of chloride ions bound at the tetramer interface, with coloring as in Figure 4. Chloride ions are shown as purple spheres. Interactions between chloride ions and protein atoms are represented as black dashed lines. Residues are labeled with their corresponding protomer in parentheses.

of each protomer (Figures 4D and 6B). As the tetrameric assembly is symmetric, each set of interactions is present four times at the interface. The L1′2′ loop of each protomer protrudes into the opposite dimer interface, generating an overall structure that resembles two gears interlocking (Figure 4D).

The residues of the four loops contribute the majority of interactions as well as 31% of the buried surface area toward formation of the tetramer (Figure 6B). In addition, four chloride ions are present at these interfaces in the $P3_2$ structure, one for each L1′2′ loop. Each of these chloride ions is located between Arg71

of one chain and Arg256 of the other, thereby stabilizing these two adjacent positive charges (Figure 6C). The L1'2' loops have no direct interactions with the FAD cofactors. However, Ala74, Gln75, Gly76, and Arg77 are positioned within 13 Å of the FAD cofactor, and a network of hydrogen bonds connects these residues to the pyrophosphate moiety and the isoalloxazine ring system of the cofactor (Figure 6B).

■ DISCUSSION

The function of AidB in the adaptive response has been a subject of debate.[16,17,19−21] With no catalytic activity reported outside of the residual IVD activity, it remains unclear if the role of AidB in the adaptive response involves the use of the bound flavin in catalysis. The flavoprotein literature reports several cases in which flavins play structural roles and are not directly involved in catalysis.[40] Glyoxylate carboligases, for example, do not appear to use their flavins to catalyze redox chemistry but instead display flavin-dependent transitions in the oligomerization state.[41,42] For both *Pseudomonas oxalaticus* and *E. coli* glyoxylate carboligases, deflavination leads to oligomer disassembly and subsequent inactivation.[41,42] With this precedent in the literature, here we investigate the possibility that FAD serves a structural role in AidB.

With the first crystal structure of AidB showing FAD bound at the AB and the CD dimer interfaces,[20] it was tempting to propose that FAD might play a structural role in the dimerization. To test this idea, deflavinated AidB (apo AidB) was generated to measure the FAD dissocation constant and to investigate whether AidB is monomeric or even unfolded without flavin. Using CD spectroscopy, we found that removal of flavin does not unfold the protein (Figure S2B of the Supporting Information), and by fluorescence quenching, we measured an apparent K_d for FAD of 402.1 ± 35.1 nM and a Hill coefficient (h) of 1.73 ± 0.21, consistent with each FAD making extensive interactions with two AidB protomers. With the knowledge that FAD binds tightly and cooperatively to AidB, along with crystal structures showing FAD engaged in numerous interactions at the AB dimer interface, AUC experiments were conducted to determine if AidB is monomeric in the absence of flavin. Surprisingly, we found that both apo *wt*AidB and apo *mt*AidB exhibit a dimeric state instead of the expected monomeric state, while holo *wt*AidB is a tetramer.

Because the AB interface is most directly affected by FAD binding (Figures 5 and 6A), we considered whether the dimeric structure of apo AidB could be represented by AC or AD dimers, such that FAD binding would yield tetramers by bringing the A protomer of AC together with the B protomer of BD to yield ABCD tetramers. To determine which protomers create the apo AidB dimers, we calculated $s_{20,w}$ values from the crystal structure and compared them to the experimental $s_{20,w}$ values for apo *wt*AidB and apo *mt*AidB. The excellent agreement between the calculated value for the AB dimer ($s_{20,w}$ of 7.0 S) with experiment ($s_{20,w}$ of 7.0 and 7.1 S) provides strong evidence that deflavinated AidB has the form of an AB dimer. Thus, even though the flavin cofactor appears to contribute stabilizing interactions to the AB dimer, our data indicate that the AB dimer interface is present even in the absence of bound flavin cofactor. In contrast, the AC and AD interfaces are disintegrated upon deflavination despite not being directly involved in flavin binding. Although an unexpected result if one considers only direct FAD−protein interactions, this result makes sense from the perspective of total buried surface area. When a contact area is small, as is the case for the AC and AD interfaces (1782 and 1319 Å², respectively), even a

few changes in hydrogen bonds or packing interactions can make a dramatic difference in interface stability, whereas when the interface is extensive, such as the case with the AB dimer (6500 Å²), hydrogen bonds and packing interactions can be lost without having an impact on stability.

With a rationale at hand for why AidB is an AB dimer in the absence of FAD, we then considered how FAD binding generates AidB tetramers when the cofactor does not appear to be directly involved in creating the tetramer interface. To more carefully evaluate the tetramer interface, it was important to obtain a crystal structure in which more than one protomer was present in the asymmetric unit. In the $P3_2$ structure presented here, the asymmetric unit contains three copies of the tetramer interface, none of which are restrained by crystallographic symmetry. With independent tetramers to analyze, we find that binding of flavin to dimers of AidB could order residues that create an intricate network of hydrogen bonds, thereby exerting a long-range stabilization on the tetramer interface (Figure 6B). Importantly, the L1'2' loops (residues 69−80) that protrude across the tetramer interface (Figure 4D) and make the majority of contacts at the interface are involved in this hydrogen bonding network. With so little buried surface area at the tetramer interface, the loss or disruption of these interactions due to the absence of FAD must be enough to shift the balance from tetramer to dimer, while the AB interface is strong enough to exist without FAD. Formation of the tetramer interface could also be dependent on ionic strength, as four chloride molecules are present at the interface, again contacting the L1'2' loop (Figure 6C). AidB remains a tetramer at NaCl concentrations as low as 100 mM (data not shown), but the instability of the protein precluded experiments at lower salt concentrations.

Notably, while AidB shares sequence homology and structural similarity with members of the ACAD family such as IVD and medium chain acyl-CoA dehydrogenase (MCAD),[16,43,44] the AidB L1'2' loop and the DNA-binding region are not conserved in any other members of the ACAD family. Presumably, as a result of these differences, the structures of IVD and MCAD reveal a completely different tetrameric arrangement compared to that observed for AidB (Figure S4 of the Supporting Information). The DNA-binding domain prevents AidB from forming the IVD-type tetramer, while the lack of the L1'2' loop in IVD would restrict the formation of an AidB-like tetramer in that protein. Thus, AidB could have diverged from the ACAD family by the addition of this DNA-binding domain, allowing it to perform its function in the adaptive response, while the addition of the L1'2' β-hairpin loop would still allow for tetramer formation. With so few alterations in the secondary structure between the ACAD family and AidB, the adaptation of the L1'2' loop suggests that tetramerization is important to the function of AidB.

We also found that the transition from a tetrameric state to a dimeric state is fully reversible and does not depend on the flavin oxidation state, as reconstitution of apo *wt*AidB by oxidized FAD restores the tetrameric state and reduced holo *wt*AidB is a tetramer. Notably, incorporation of free FAD into apo *wt*AidB is a highly cooperative process as indicated by both AUC and fluorescence quenching studies. During stepwise reconstitution experiments, regardless of the amount of FAD used, all FAD-containing AidB molecules are tetramers. Although we cannot predict the exact mechanism of tetramerization, all of these results support a model in which binding of substoichiometric amounts of FAD promotes

tetramer formation for *wt*AidB. Thus, while the individual structures of AidB protomers are likely to be retained during deflavination, we observe a reversible and flavin-dependent change in the oligomeric state, indicating that flavin, regardless of oxidation state, does play a structural role in the creation of the AidB tetramer.

Despite the switch in oligomeric state upon deflavination, the in vitro DNA binding capability of apo AidB was not significantly affected, with a <2-fold effect compared to that of holo AidB. These results also suggest that tetramerization is not essential for the interaction of AidB with double-stranded DNA. In agreement with these findings, it was recently reported that a truncated version of AidB that contains only the DNA-binding domain, and thus is unlikely to be tetrameric, retains the capability of binding DNA in vitro.[21] In vivo, however, tetramerization could allow AidB to bind DNA at multiple locations simultaneously.

Interestingly, the higher-order AidB oligomer observed in the *I*222 crystal structure and proposed to sequester and thereby protect DNA[20] is not present in the *P*3$_2$ crystal form, nor do we observe any higher-order AidB oligomers in our solution studies. The distinct architecture of the crystal lattice could be due to the absence of DNA under our crystallization conditions; however, no electron density for DNA was observed in the previously reported structure.[20] More likely, AidB can crystallize in multiple lattice systems, as is frequently observed for other proteins (for examples, see refs 45 or 46 and 47), with these two AidB crystal structures representing two of the possible lattice systems. While an AidB "mega complex" exists at least in the *I*222 crystal lattice, a role for this complex in sequestering DNA is not supported by our studies. With respect to the idea of protection by DNA sequestration in general, recent data from the Volkert laboratory oppose this model.[17] Their data show that deletion of AidB's DNA-binding domain does not result in the loss of AidB's protective function; the protective ability is independent of DNA binding.[17] Protection in the absence of DNA binding is also inconsistent with AidB serving as a DNA repair protein. While our studies clearly show FAD-dependent oligomerization of AidB, they do not address whether FAD also has a catalytic function. However, the picture of AidB that is emerging invokes a role for the DNA-binding domain in localization of AidB to specific genes, while the protective function appears to reside elsewhere on the protein.[17,21] Whether this protective function resides with FAD or whether FAD was retained in the evolutionary process solely for its ability to stabilize the AidB tetramer remains to be determined.

ASSOCIATED CONTENT

⑤ Supporting Information

Primers for site-directed mutagenesis, crystallographic data collection and refinement statistics, UV–vis and CD spectra of different AidB forms, and additional figures of the crystal structure. This material is available free of charge via the Internet at http://pubs.acs.org.

Accession Codes

The atomic coordinates have been deposited with the Protein Data Bank as entry 3U33.

AUTHOR INFORMATION

Corresponding Author

*S.J.E.: telephone, (617) 358-2816; fax, (617) 353-6466; e-mail, elliott@bu.edu. C.L.D.: telephone, (617) 253-5622; fax, (617) 258-7847; e-mail, cdrennan@mit.edu.

Present Address

@Johnson & Johnson Pharmaceutical Research & Development, 930 Route 202 South, Raritan, NJ 08869.

Author Contributions

M.J.H. and M.J. contributed equally to this work.

ABBREVIATIONS

MNNG, *N*-methyl-*N'*-nitro-*N*-nitrosoguanidine; FAD, flavin adenine dinucleotide; ACAD, acyl-coenzyme A dehydrogenase; IVD, isovaleryl-coenzyme A dehydrogenase; K_d, dissociation constant; *β*-ME, *β*-mercaptoethanol; EDTA, ethylenediaminetetraacetic acid; *h*, Hill coefficient; NCS, noncrystallographic symmetry; CD, circular dichroism; AUC, analytical ultracentrifugation; $s_{20,w}$, sedimentation coefficient normalized to 20 °C and water; rmsd, root-mean-square deviation; MCAD, medium chain acyl-coenzyme A dehydrogenase.

REFERENCES

(1) Sedgwick, B. (2004) Repairing DNA-methylation damage. *Nat. Rev. Mol. Cell Biol.* 5, 148−157.

(2) Volkert, M. R., and Nguyen, D. C. (1984) Induction of specific *Escherichia coli* genes by sublethal treatments with alkylating agents. *Proc. Natl. Acad. Sci. U.S.A.* 81, 4110−4114.

(3) Volkert, M. R. (1988) Adaptive response of *Escherichia coli* to alkylation damage. *Environ. Mol. Mutagen.* 11, 241−255.

(4) Samson, L., and Cairns, J. (1977) A new pathway for DNA repair in *Escherichia coli*. *Nature* 267, 281−283.

(5) Sedgwick, B., Robins, P., Totty, N., and Lindahl, T. (1988) Functional domains and methyl acceptor sites of the *Escherichia coli* Ada protein. *J. Biol. Chem.* 263, 4430−4433.

(6) Demple, B., Sedgwick, B., Robins, P., Totty, N., Waterfield, M. D., and Lindahl, T. (1985) Active site and complete sequence of the suicidal methyltransferase that counters alkylation mutagenesis. *Proc. Natl. Acad. Sci. U.S.A.* 82, 2688−2692.

(7) Landini, P., and Volkert, M. R. (2000) Regulatory responses of the adaptive response to alkylation damage: A simple regulon with complex regulatory features. *J. Bacteriol.* 182, 6543−6549.

(8) Sedgwick, B., and Lindahl, T. (2002) Recent progress on the Ada response for inducible repair of DNA alkylation damage. *Oncogene 21*, 8886−8894.

(9) Evensen, G., and Seeberg, E. (1982) Adaptation to alkylation resistance involves the induction of a DNA glycosylase. *Nature 296*, 773−775.

(10) Karran, P., Hjelmgren, T., and Lindahl, T. (1982) Induction of a DNA glycosylase for *N*-methylated purines is part of the adaptive response to alkylating agents. *Nature 296*, 770−773.

(11) Trewick, S. C., Henshaw, T. F., Hausinger, R. P., Lindahl, T., and Sedgwick, B. (2002) Oxidative demethylation by *Escherichia coli* AlkB directly reverts DNA base damage. *Nature 419*, 174−178.

(12) Falnes, P. O., Johansen, R. F., and Seeberg, E. (2002) AlkB-mediated oxidative demethylation reverses DNA damage in *Escherichia coli*. *Nature 419*, 178−182.

(13) Falnes, P. O. (2004) Repair of 3-methylthymine and 1-methylguanine lesions by bacterial and human AlkB proteins. *Nucleic Acids Res. 32*, 6260.

(14) Delaney, J. C., Smeester, L., Wong, C., Frick, L. E., Taghizadeh, K., Wishnok, J. S., Drennan, C. L., Samson, L. D., and Essigmann, J. M. (2005) AlkB reverses etheno DNA lesions caused by lipid oxidation in vitro and in vivo. *Nat. Struct. Mol. Biol. 12*, 855−860.

(15) Frick, L. E., Delaney, J. C., Wong, C., Drennan, C. L., and Essigmann, J. M. (2007) Alleviation of 1,N^6-ethanoadenine genotoxicity by the *Escherichia coli* adaptive response protein AlkB. *Proc. Natl. Acad. Sci. U.S.A. 104*, 755−760.

(16) Landini, P., Hajec, L. I., and Volkert, M. R. (1994) Structure and transcriptional regulation of the *Escherichia coli* adaptive response gene aidB. *J. Bacteriol. 176*, 6583−6589.

(17) Rippa, V., Duilio, A., di Pasquale, P., Amoresano, A., Landini, P., and Volkert, M. R. (2011) Preferential DNA damage prevention by the *E. coli* AidB gene: A new mechanism for the protection of specific genes. *DNA Repair 10*, 934−941.

(18) Volkert, M. R., Nguyen, D. C., and Beard, K. C. (1986) *Escherichia coli* gene induction by alkylation treatment. *Genetics 112*, 11−26.

(19) Rohankhedkar, M. S., Mulrooney, S. B., Wedemeyer, W. J., and Hausinger, R. P. (2006) The AidB component of the *Escherichia coli* adaptive response to alkylating agents is a flavin-containing, DNA-binding protein. *J. Bacteriol. 188*, 223−230.

(20) Bowles, T., Metz, A. H., O'Quin, J., Wawrzak, Z., and Eichman, B. F. (2008) Structure and DNA binding of alkylation response protein AidB. *Proc. Natl. Acad. Sci. U.S.A. 105*, 15299−15304.

(21) Rippa, V., Amoresano, A., Esposito, C., Landini, P., Volkert, M., and Duilio, A. (2010) Specific DNA binding and regulation of its own expression by the AidB protein in *Escherichia coli*. *J. Bacteriol. 192*, 6136−6142.

(22) Mulrooney, S. B., Howard, M. J., and Hausinger, R. P. (2011) The *Escherichia coli* alkylation response protein AidB is a redox partner of flavodoxin and binds RNA and acyl carrier protein. *Arch. Biochem. Biophys. 513*, 81−86.

(23) Kelly, S. M., Jess, T. J., and Price, N. C. (2005) How to study proteins by circular dichroism. *Biochim. Biophys. Acta 1751*, 119−139.

(24) Curley, G. P., Carr, M. C., Mayhew, S. G., and Voordouw, G. (1991) Redox and flavin-binding properties of recombinant flavodoxin from *Desulfovibrio vulgaris* (Hildenborough). *Eur. J. Biochem. 202*, 1091−1100.

(25) Laue, T. M., Shah, B. D., Ridgeway, T. M., and Pelletier, S. L. (1992) Computer-aided interpretation of analytical sedimentation data for proteins. In *Analytical ultracentrifugation in biochemistry and protein science* (Harding, S. E., Rowe, A. J., and Horton, J. C., Eds.) pp 90−125, Royal Society of Chemistry, Cambridge, U.K.

(26) Garcia De La Torre, J., Huertas, M. L., and Carrasco, B. (2000) Calculation of hydrodynamic properties of globular proteins from their atomic-level structure. *Biophys. J. 78*, 719−730.

(27) Lebowitz, J., Lewis, M. S., and Schuck, P. (2002) Modern analytical ultracentrifugation in protein science: A tutorial review. *Protein Sci. 11*, 2067−2079.

(28) Philo, J. S. (2000) A method for directly fitting the time derivative of sedimentation velocity data and an alternative algorithm for calculating sedimentation coefficient distribution functions. *Anal. Biochem. 279*, 151−163.

(29) Otwinowski, Z., and Minor, W. (1997) Processing of X-ray diffraction data collected in oscillation mode. In *Methods in Enzymology* (Carter, C. W., Jr., and Sweet, R. M., Eds.) pp 307−326, Academic Press, New York.

(30) McCoy, A. J., Grosse-Kunstleve, R. W., Adams, P. D., Winn, M. D., Storoni, L. C., and Read, R. J. (2007) Phaser crystallographic software. *J. Appl. Crystallogr. 40*, 658−674.

(31) Brunger, A. T., Adams, P. D., Clore, G. M., DeLano, W. L., Gros, P., Grosse-Kunstleve, R. W., Jiang, J. S., Kuszewski, J., Nilges, M., Pannu, N. S., Read, R. J., Rice, L. M., Simonson, T., and Warren, G. L. (1998) Crystallography & NMR system: A new software suite for macromolecular structure determination. *Acta Crystallogr. D54*, 905−921.

(32) Brunger, A. T. (2007) Version 1.2 of the Crystallography and NMR system. *Nat. Protoc. 2*, 2728−2733.

(33) Emsley, P., Lohkamp, B., Scott, W. G., and Cowtan, K. (2010) Features and development of Coot. *Acta Crystallogr. D66*, 486−501.

(34) Adams, P. D., Afonine, P. V., Bunkoczi, G., Chen, V. B., Davis, I. W., Echols, N., Headd, J. J., Hung, L. W., Kapral, G. J., Grosse-Kunstleve, R. W., McCoy, A. J., Moriarty, N. W., Oeffner, R., Read, R. J., Richardson, D. C., Richardson, J. S., Terwilliger, T. C., and Zwart, P. H. (2010) PHENIX: A comprehensive Python-based system for macromolecular structure solution. *Acta Crystallogr. D66*, 213−221.

(35) Painter, J., and Merritt, E. A. (2006) Optimal description of a protein structure in terms of multiple groups undergoing TLS motion. *Acta Crystallogr. D62*, 439−450.

(36) Chen, V. B., Arendall, W. B. III, Headd, J. J., Keedy, D. A., Immormino, R. M., Kapral, G. J., Murray, L. W., Richardson, J. S., and Richardson, D. C. (2010) MolProbity: All-atom structure validation for macromolecular crystallography. *Acta Crystallogr. D66*, 12−21.

(37) *The PyMOL Molecular Graphics System*, version 1.3r1 (2010) Schrodinger, LLC, New York.

(38) Hefti, M. H., Vervoort, J., and van Berkel, W. J. (2003) Deflavination and reconstitution of flavoproteins. *Eur. J. Biochem. 270*, 4227−4242.

(39) Krissinel, E., and Henrick, K. (2007) Inference of macro-molecular assemblies from crystalline state. *J. Mol. Biol. 372*, 774−797.

(40) Bornemann, S. (2002) Flavoenzymes that catalyse reactions with no net redox change. *Nat. Prod. Rep. 19*, 761−772.

(41) Chung, S. T., Tan, R. T., and Suzuki, I. (1971) Glyoxylate carboligase of *Pseudomonas oxaliticus*. A possible structural role for flavine-adenine dinucleotide. *Biochemistry 10*, 1205−1209.

(42) Cromartie, T. H., and Walsh, C. T. (1976) *Escherichia coli* glyoxalate carboligase. Properties and reconstitution with 5-deazaFAD and 1,5-dihydrodeazaFADH$_2$. *J. Biol. Chem. 251*, 329−333.

(43) Tiffany, K. A., Roberts, D. L., Wang, M., Paschke, R., Mohsen, A. W., Vockley, J., and Kim, J. J. P. (1997) Structure of human isovaleryl-CoA dehydrogenase at 2.6 Å resolution: Basis for substrate specificity. *Biochemistry 36*, 8455−8464.

(44) Kim, J. J., Wang, M., and Paschke, R. (1993) Crystal structures of medium-chain acyl-CoA dehydrogenase from pig liver mitochondria with and without substrate. *Proc. Natl. Acad. Sci. U.S.A. 90*, 7523−7527.

(45) Higgins, L. J., Yan, F., Liu, P. H., Liu, H. W., and Drennan, C. L. (2005) Structural insight into antibiotic fosfomycin biosynthesis by a mononuclear iron enzyme. *Nature 437*, 838−844.

(46) Nordlund, P., Sjoberg, B. M., and Eklund, H. (1990) 3-Dimensional Structure of the Free-Radical Protein of Ribonucleotide Reductase. *Nature 345*, 593−598.

(47) Sommerhalter, M., Saleh, L., Bollinger, J. M., and Rosenzweig, A. C. (2005) Structure of *Escherichia coli* ribonucleotide reductase R2 in space group P6$_1$22. *Acta Crystallogr. D61*, 1649−1654.